

PCCP

Accepted Manuscript



This is an *Accepted Manuscript*, which has been through the Royal Society of Chemistry peer review process and has been accepted for publication.

Accepted Manuscripts are published online shortly after acceptance, before technical editing, formatting and proof reading. Using this free service, authors can make their results available to the community, in citable form, before we publish the edited article. We will replace this *Accepted Manuscript* with the edited and formatted *Advance Article* as soon as it is available.

You can find more information about *Accepted Manuscripts* in the [Information for Authors](#).

Please note that technical editing may introduce minor changes to the text and/or graphics, which may alter content. The journal's standard [Terms & Conditions](#) and the [Ethical guidelines](#) still apply. In no event shall the Royal Society of Chemistry be held responsible for any errors or omissions in this *Accepted Manuscript* or any consequences arising from the use of any information it contains.

Polaronic effects at finite temperatures in the B850 ring of LH2 complex

Vladimir Chorošajev, Olga Rancova, and Darius Abramavicius*

Received Xth XXXXXXXXXXXX 20XX, Accepted Xth XXXXXXXXXXXX 20XX

First published on the web Xth XXXXXXXXXXXX 200X DOI: 10.1039/b000000x

Energy transfer and relaxation dynamics in the B850 ring of LH2 molecular aggregate are described, taking into account the polaronic effects, by a stochastic time-dependent variational approach. We explicitly include the finite temperature effects into the model by sampling the initial conditions of the vibrational states randomly. This is in contrast to previous applications of the variational approach, which consider only the zero-temperature case. The method allows us to obtain both the microscopic dynamics at the single-wavefunction level and the thermally averaged picture of excitation relaxation in a wide range of temperatures. Spectroscopic observables such as temperature dependent absorption and time-resolved fluorescence spectra are calculated. Microscopic wavefunction evolution is quantified by introducing the exciton participation (localization) length and exciton coherence length. Their asymptotic temperature dependence demonstrates that the environmental polaronic effects range from exciton self-trapping and excitonic polaron formation at low temperatures to thermally induced state delocalization and decoherence at high temperatures. While this is observed on wavefunction level it remains hidden spectroscopically.

1 Introduction

Delocalized electronic excitations of optically active molecular complexes and aggregates are usually described within the framework of exciton theory¹. The length scales of such systems grant them properties similar both to single molecules and to solid state. Such systems show unique electronic and optical properties. They display features of discrete transitions as opposed to continuous bands of bulk materials, yet their coherent excitations are delocalized over multiple constituent monomers. The importance of theoretical and experimental studies of the aggregates has steadily increased throughout the last decade. Prospective uses of artificially created aggregates include solar cells and photochemical functional complexes, while Nature utilizes them in primary processes of photosynthesis².

A set of approximations is commonly used when trying to model the electronic excitation dynamics in such systems theoretically³. Their dynamics are very strongly dependent on interactions with the local intramolecular vibrations and their immediate surroundings usually referred to as the phonon bath^{4,5}. Consequently the electric dipole moments of the excited states may cause non-uniform polarization of the immediate environment, creating excitonic polarons⁶. This presents a serious challenge for describing the collective dynamics and decoherence effects. For instance, in photosynthetic aggregates¹ the couplings between monomers can be of the same

order as couplings to vibrations, which makes the perturbation theory a rough approximation. Additionally, the very spectral content of the environment vibrations is very complex and is difficult to predict theoretically and just as difficult to measure experimentally, requiring hole-burning, Raman and fluorescence line narrowing experiments^{7,8}. Even then, the model parameters may vary between monomers in the same system, dependent on their respective place in the protein matrix causing inhomogeneous disorder. On the other hand, there is a huge amount of spectroscopic information available for some of these naturally occurring molecular aggregates, including coherent multi-dimensional spectroscopy that directly measures the nonlinear optical response of the system and reveals homogeneous and inhomogeneous linewidths⁹. This gives the possibility to fix some model parameters with confidence.

One of the basic light harvesting agents in studies of photosynthesis is the LH2 - the peripheral light harvesting complex of purple bacteria^{10,11}. The complex demonstrates outstandingly high circular symmetry and the atomic structure obtained by X-ray crystallography¹² is known for two bacteria species: *Rhodospirillum rubrum*¹³ and *Rhodospirillum rubrum*^{14,15} (now *Rhodospirillum rubrum*¹⁶). The latter complex consists of 27 bacteriochlorophyll (BChl) *a* pigments bound to a protein matrix and arranged in two concentric C_9 -symmetry rings: one having 9 pigments and the other 18. The complex has two prominent absorption bands at 800nm and 850nm at room temperature. The rings are commonly associated with these absorption peaks and named correspondingly to their absorption maxima (in nanometers) as B800 and B850. The 9 Bchl *a* pigments that compose

Department of Theoretical Physics, Faculty of Physics, Vilnius University, Saulėtekio Ave. 9, build. 3, LT-10222 Vilnius, Lithuania

* E-mail: darius.abramavicius@ff.vu.lt

the B800 ring are weakly interacting, and the B850 ring is grouped into 9 strongly interacting heterodimeric pairs of Bchl *a* pigments^{17–23}. The lowest-energy optical transition of isolated Bchl *a* pigments raises a peak approximately at 770nm (dependent on solvent), and the large shift in transition frequency of LH2 is caused by the excitonic splitting and the reorganization of the local environment. Frenkel exciton model has been successful to explain absorption spectroscopy^{11,24,25} as well as ultrafast dephasing in two dimensional coherent spectroscopy experiments^{26–29} showing the relevance of *k*-band electronic structure^{30–32}. However, the temperature dependencies of the spectra require to include dichotomous corrections^{33,34}, or more complex anharmonic phonon properties²⁹. Simulations of the experimental emission spectra of LH2 suggested that the exciton model is not enough to explain the broadening of the lowest exciton state and the temperature dependence of the fluorescence lifetime. Exciton self-trapping in the B850 ring has been suggested to explain the effects^{21,35,36}. The same concept of exciton self-trapping has been used to explain the experimental data on site-selective spectra³⁷ and single-complex fluorescence excitation and emission spectra³⁸.

However, the polaronic effects are not trivial to confirm at ambient temperature because superpositions of states are in play. It has been shown in ref.³⁹ that the off-diagonal elements of the density matrix not decaying to zero asymptotically corresponds to non-optimal choice of representation (quantum mechanical basis set). According to the statistical physics the thermal equilibrium density operator in the global eigenstate basis is necessarily diagonal, i. e. the off-diagonal elements of the density matrix are zero. The search for polaronic effects then corresponds to the search of the global eigenbasis (also known as the pointer basis set of the system undergoing decoherence)^{40,41} and comparing it to the excitonic basis. The excitonic polaron picture has been demonstrated to be relevant in the case of overdamped phonon bath at an arbitrary temperature in a model system^{39,42}.

Redfield relaxation theory does not account for polaron effects. There is a number of theoretical methods available for description of the intermediate excitonic-vibrational coupling regime, where non-perturbative treatment is needed, though they come with additional costs. The exact hierarchical equations of motion approach describes the excited state evolutions precisely³⁹, however, it imposes restrictions on the spectral content of vibrations and the computation time scales unfavorably with the number of system sites, making it difficult to apply to large molecular aggregates. Methods based on time-dependent version of density matrix reorganization groups are applicable only to one-dimensional systems⁴³. In this paper we describe excitation dynamics and trapping in the strongly coupled B850 ring of LH2 aggregate utilizing the non-perturbative quantum variational approach to the

wavefunction of the excitonic system based on the Davydov Ansatz^{44–48}. We additionally extend the conventional zero-temperature approach by introducing stochastic initial conditions of the vibrational modes, thus introducing finite temperatures. The approach results in a nonlinear set of equations for the excitonic wavefunction and hence includes the branching dynamics of nonlinear systems, i. e., the exciton-polaron transitions. The exciton wave-like propagation, self-trapping and delocalization effects in this ring are obtained and characterized via simulations of excitation relaxation dynamics together with linear absorption / fluorescence spectra.

2 Theory

Excitations in the pigment-protein aggregates are usually considered as Frenkel excitons delocalized over several pigments^{1,3,49}. While the molecules may be identical in their chemical composition, the conformational disorder breaks the symmetries. Additionally, molecular vibrations perturb the energies of electronic transitions. Thus we apply the model including the static and time-dependent site energy variation, described by the following Holstein Hamiltonian:

$$\hat{H} = \sum_n (\varepsilon_n + \delta_n) \hat{a}_n^\dagger \hat{a}_n + \sum_{m \neq n} J_{mn} \hat{a}_m^\dagger \hat{a}_n + \sum_q \omega_q \hat{b}_q^\dagger \hat{b}_q - \sum_n \hat{a}_n^\dagger \hat{a}_n \sum_q g_{qn} \omega_q (\hat{b}_q^\dagger + \hat{b}_q). \quad (1)$$

Here ε_n denotes the average electronic transition energy for site n and δ_n is the static (random) transition energy shift specific for each different member of the total statistical ensemble. J_{mn} is the resonant coupling matrix element between sites m and n . \hat{a}_n^\dagger and \hat{a}_n are the creation and annihilation operators for an electronic excitation at site n , \hat{b}_q^\dagger and \hat{b}_q are the creation and annihilation operators for the vibrational modes (including modes belonging to the phonon field), q is the mode index, ω_q is its frequency (we set $\hbar = 1$), and g_{qn} is the linear coupling strength between the site n and the phonon mode q . The total energy of the system is shifted by a constant $-\frac{1}{2} \sum_q \omega_q$ value of all-phonon zero-point energy, which makes no difference for the spectroscopic observables. The static energy shifts δ_n are responsible for diagonal static disorder: the values are randomly chosen according to a Gaussian probability distribution with zero mean and standard deviation σ_n . Different site energy disorder values are uncorrelated.

Microscopic excitation dynamics are obtained by applying the Dirac-Frenkel variational principle⁵⁰ to a certain trial wavefunction, which corresponds to the Davydov D_2 Ansatz^{45,46}:

$$|\Psi_{D_2}(t)\rangle = \sum_n \left(\alpha_n(t) \hat{a}_n^\dagger \exp\left[\sum_q \lambda_q(t) \hat{b}_q^\dagger - \text{h.c.}\right] \right) |0\rangle_e |0\rangle_p. \quad (2)$$

This procedure optimizes the Ansatz so that the deviation from the exact solution of the Schrödinger equation is minimal. Accordingly, an arbitrary vibrational non-equilibrium state of such a system is described by a single multidimensional coherent state, displaced by $\lambda_q(t)$ (for mode q) from its origin in coordinate-momentum phase space. This approach allows us to treat very large numbers of vibrational modes explicitly, avoiding the reduced density operator approach. Electronic excitation states $\alpha_n(t)$ span the whole single-excitation subspace. The bath subspace of the solutions is limited to a subspace spanned by the parametrized Ansatz. In this parametrization the vibrational wavefunction of a single oscillator is always given by a single coherent state (superposition of such states in a single oscillator is not included), and the excitonic subspace of the parametrized solution admits an arbitrary single-excitation state. Considering N sites and Q total modes for the phonon field, the wavefunction then requires $N + Q$ complex time-dependent parameters to be uniquely specified. The phonon amplitudes are independent of the electronic state amplitudes in the D_2 Ansatz (in contrast to the Davydov D_1 Ansatz), but the local bath correlates the amplitudes in the resulting equations of motion. We denote the projections of the trial wavefunction to electronic and vibrational subspaces as $|\Psi_{D_2}(t)\rangle_e$ and $|\Psi_{D_2}(t)\rangle_p$.

In order to obtain the $\alpha(t)$ and $\lambda(t)$ functions that would minimize the deviation from the exact solution, we closely follow the procedure given in⁴². In our previous paper we used a more complicated Ansatz form and studied only the zero-temperature case. However, the simpler Davydov D_2 Ansatz as the trial wavefunction as used in this paper still captures polaronic dynamics. Additionally, the simpler equations of motion allow faster computation and thus allow random sampling of bath states, which is used to account for finite temperature. The detailed derivation of the present model is given in Appendix A. The resulting equations of motion are:

$$\dot{\alpha}_n = -i\alpha_n \sum_m |\alpha_m|^2 z_m(t) - i(\varepsilon_n + \delta_n) \alpha_n \quad (3)$$

$$- i \sum_{m \neq n} J_{nm} \alpha_m + i\alpha_n z_n(t),$$

$$\dot{\lambda}_q = -i\omega_q \lambda_q + i \sum_n |\alpha_n|^2 g_{qn} \omega_q, \quad (4)$$

where

$$z_n(t) = \sum_q g_{qn} \omega_q (\lambda_{qn} + \lambda_{qn}^*) \quad (5)$$

is the real-valued collective coordinate function. At high temperature for the large number of modes forming a smooth spectral density function shape, the collective coordinates (Eqn. 5) perform classical Gaussian fluctuations. This approach results in an initial value problem that can be solved us-

ing common methods. Here we use the adaptive step Runge-Kutta (4,5) algorithm for the numerical solution.

We make a widely used assumption that the length scale of the phonon modes is much smaller than the distance between pigments in a molecular aggregate and consider the modes to be localized and coupled only to a single site, making the fluctuations of the site energies uncorrelated. Technically, we set the coupling constants in such a way that a site only interacts with a subset of the environmental oscillators. Hence, the total oscillator number $Q = Q_{\text{site}}N$, where Q_{site} is the number of oscillators interacting with a single site. Then for a site n the coupling constants $g_{qn} \neq 0$ only for $nQ_{\text{site}} \leq q < (n+1)Q_{\text{site}}$. Hence, each oscillator becomes coupled with a single specific pigment. This assumption allows us to define the spectral density function of a site n ³:

$$C_n''(\omega) = \pi \sum_q g_{qn}^2 \omega_q^2 \delta(\omega - \omega_q). \quad (6)$$

Integrating it over the complete range of frequencies, we obtain the reorganization energies of the sites:

$$\Lambda_n = \frac{1}{\pi} \int_0^\infty \frac{C_n''(\omega)}{\omega} d\omega = \sum_q g_{qn}^2 \omega_q. \quad (7)$$

In real systems the number of environmental modes is effectively infinite, making the spectral density a continuous function (though sharp peaks corresponding to specific intramolecular vibrational modes are prominent at higher frequencies).

The system being at constant temperature must contain thermal energy in all vibrational modes. Hence, the temperature of the environment determines the energy and displacements of the vibrational modes. The phonons prior to optical excitation of the system are in thermal equilibrium and hence can be sampled from a thermal state. The equilibrium density operator of a thermal state is the canonical ensemble:

$$\hat{\rho} = \frac{1}{\mathcal{Z}} \exp \left(- \frac{\sum_q \omega_q (\hat{b}_q^\dagger \hat{b}_q + \frac{1}{2})}{kT} \right). \quad (8)$$

Using the Glauber-Sudarshan P representation of the equilibrium thermal state⁵¹ the density operator in a coherent state basis is given by

$$\hat{\rho} = \sum_q \int P_q(\lambda_q) |\lambda_q\rangle \langle \lambda_q| d\text{Re} \lambda_q d\text{Im} \lambda_q, \quad (9)$$

where $P_q(\lambda)$ is a generalized probability distribution for each vibrational mode. The $P_q(\lambda)$ function is equal to:

$$P_q(\lambda) = \mathcal{Z}^{-1} \exp \left(-|\lambda_q|^2 \exp \left[-\frac{\omega_q}{kT} \right] \right), \quad (10)$$

where \mathcal{Z} is the partition function of a single oscillator. Consequently, the initial conditions for the environmental phonon states prior to optical excitation are sampled from distribution (10). Note that the mean energy of a phonon mode sampled using the provided $P_q(\lambda)$ function is equal to $\frac{1}{2}\omega_q \coth \frac{\omega_q}{2kT}$, so the high frequency modes of the system are at ground state prior to the optical excitation. This is the only way the temperature comes in when determining the dynamics of the system. The zero temperature case then corresponds to every environmental oscillator being in the ground state initially (which is exactly equivalent to a coherent state with displacement parameter $\lambda_q = 0$).

For the spectroscopy simulations presented in this paper we model the absorption and emission events using a broadband optical pulse (ideally of an infinitely small duration and infinitely broad spectrum). The elementary optical excitation event (in the sense of perturbation theory) is then realized by acting with the system-field interaction Hamiltonian, $\hat{H}_{SF} = \hat{d} \cdot \mathbf{E}$ with $\hat{d} = \sum_n \boldsymbol{\mu}_n (\hat{a}_n^\dagger + \hat{a}_n)$, on the electronic ground state leading to the initial excited state

$$|\Psi_{D2}(0)\rangle_e \equiv \mathcal{N}^{-1} \sum_n (\boldsymbol{\mu}_n \cdot \mathbf{E}) \hat{a}_n^\dagger |0\rangle_e \quad (11)$$

with \mathbf{E} being the electric field vector, $\boldsymbol{\mu}_n$ the site transition dipole vector, \mathcal{N} the normalization of the wavefunction. The direction of the electric field is generated randomly for each realization to account for an arbitrary orientation. This excitation defines the initial conditions for the electronic subsystem and takes into account the orientational properties of the site dipoles.

The observables of interest are the absorption and time-resolved fluorescence spectra, the occupation probabilities of individual sites or groups of sites and the delocalization length of the excitation. The absorption spectrum is obtained from the linear response theory by calculating the time-domain response functions and averaging over the realizations of both the static disorder and randomly sampled initial conditions for the vibrational states. Using the wavefunction approach we have the following form for the linear absorption⁵²:

$$F^{\text{abs}}(\omega) = \text{Re} \int_{-\infty}^{\infty} dt e^{i\omega t} \sum_R \mathcal{F}_R^{\text{abs}}(t), \quad (12)$$

where $\mathcal{F}_R(t)$ is the linear optical response function for a single fluctuating trajectory R . It can be explicitly evaluated in terms

of dynamical variables α_n, λ_q (Eqns. 3,4) as:

$$\begin{aligned} \mathcal{F}_R^{\text{abs}}(t) &= \langle \Psi_{D2}(0) | \hat{p} | 0 \rangle \langle 0 | \hat{d} e^{i\hat{H}_B t} | \Psi_{D2}(t) \rangle \\ &= \sum_{m,n} (\boldsymbol{\mu}_m \cdot \boldsymbol{\mu}_n) \alpha_m^*(0) \alpha_n(t) \\ &\quad \cdot \exp \sum_q \left(e^{i\omega_q t} \lambda_q^*(0) \lambda_q(t) \right. \\ &\quad \left. - \frac{1}{2} [|\lambda_q(0)|^2 + |\lambda_q(t)|^2] \right), \end{aligned} \quad (13)$$

with $\hat{H}_B = \sum_q \omega_q \hat{b}_q^\dagger \hat{b}_q$. The time-resolved auxiliary fluorescence optical response function⁵³ is calculated similarly:

$$F^{\text{trf}}(\omega, \tau) = \text{Re} \int_{-\infty}^{\infty} dt e^{i\omega t} \sum_R \mathcal{F}_R^{\text{trf}}(t, \tau), \quad (14)$$

where the contribution from a single realization is given by

$$\begin{aligned} \mathcal{F}_R^{\text{trf}}(t, \tau) &= \langle \Psi_{D2}(\tau) | \hat{d} e^{i\hat{H}_B t} \hat{d} | \Psi_{D2}(t) \rangle \\ &= \mathcal{S}_R \cdot \sum_{m,n} (\boldsymbol{\mu}_m \cdot \boldsymbol{\mu}_n) \alpha_m^*(\tau) \alpha_n(t) \\ &\quad \cdot \exp \sum_q \left(e^{i\omega_q(t-\tau)} \lambda_q^*(\tau) \lambda_q(t) \right. \\ &\quad \left. - \frac{1}{2} [|\lambda_q(\tau)|^2 + |\lambda_q(t)|^2] \right), \end{aligned} \quad (15)$$

with $\mathcal{S}_R = \sum_n (\mathbf{E} \cdot \boldsymbol{\mu}_n)^2$ being the weight factor for the realization characterizing its excitation probability. This expression is analogous to absorption except the time arguments are shifted to allow the partial equilibration in the electronic excited state for a time period τ .

3 Model parameters of LH2 aggregate

The above described model is used to describe excitation dynamics of photosynthetic LH2 aggregate. We choose to investigate separately some observables of the full LH2 system, and then focus on the excitation dynamics of the B850 ring. The site energy and coupling matrix (the Hamiltonian of the electronic subsystem) is used as described in Ref.^{25,29}. Additionally we average energies of identical pigments: B800, α -B850, and β -B850; where α -B850 and β -B850 refer to the pigments bound to the α (outer) and β (inner) transmembrane proteins of LH2 complex respectively. In the model the site energies of α -B850 pigments are about 310 cm^{-1} higher than of β -B850. The site-dependent conformational disorder δ_n was generated according to a Gaussian distribution with standard deviations: $\sigma_{B800} = 60 \text{ cm}^{-1}$, $\sigma_{B850} = 220 \text{ cm}^{-1}$, where σ_{B800} is the value for every pigment belonging to the B800 ring, and σ_{B850} for every pigment belonging to the B850 ring²⁹.

The form for the spectral density function was chosen as a sum of Ohmic and super-Ohmic spectral densities to correctly account for the low-frequency behaviour⁵⁴, which is the most relevant for intra-ring energy transfer. The bath parameters are assumed from experimental absorption lineshape studies⁵⁵:

$$C_n''(\omega) = \sum_{i=1}^2 \omega^{i+1} e^{-\frac{\omega}{\omega_{c,i}}} \frac{\alpha_i}{\omega_{c,i}^i (i+1)!}. \quad (16)$$

Here $\omega_{c,1} = 50 \text{ cm}^{-1}$, $\omega_{c,2} = 15 \text{ cm}^{-1}$, $\alpha_1 = 1$, $\alpha_2 = 2$. $\Lambda_{B800} = 45 \text{ cm}^{-1}$, $\Lambda_{B850} = 135 \text{ cm}^{-1}$ denote the reorganization energies (Eqn. 7) of pigments belonging to B800 and B850 rings respectively. We must note that the chosen form of spectral density function with the specified parameters does not account for the inter-ring energy transfer processes, since the spectral density approaches zero at frequencies that correspond to the energy gaps between the B800 and the B850 excitons. Additional high frequency modes may be necessary for the inter-ring relaxation⁴.

For simulations, the vibrational modes of each site are defined by uniformly discretizing the spectral density function with a frequency step Δ_ω in the frequency range $(0, W]$, where $W = \Delta_\omega Q_{\text{site}}$ is the bandwidth. W should be chosen to be larger than all relevant vibrational frequencies of the system (essentially it should match the frequency of the highest vibrational mode which is coupled to the electronic states strongly enough to influence its dynamics), while the minimum frequency interval Δ_ω defines a recurrence timescale equal to $2\pi/\Delta_\omega$. In general the latter should be larger than an arbitrary timescale of interest in the system dynamics. The phonon bandwidth (cutoff parameter W) was set to 425 cm^{-1} , while $Q_{\text{site}} = 200$ and consequently $\Delta_\omega = 2.125 \text{ cm}^{-1}$. The coupling strengths are assigned using Eqn. (6): $g_{qn}^2 \propto C_n''(\omega_q)/\omega_q^2$. The sign of g_{qn} remains arbitrary, so we keep it positive, while the values are normalized using the definition of the reorganization energy (Eqn. 7). Every simulation is averaged over 25000 realizations of static disorder and initial conditions for the vibrational states.

To investigate the localization behaviour of the excitonic states we use three quantities. The first one is the exciton participation ratio which is defined as:

$$L(t) = \langle \mathcal{S}_R \cdot \left(\sum_n |\alpha_n(t)|^4 \right)_R^{-1} \rangle, \quad (17)$$

here angular brackets denote the averaging over thermal ensemble and over disorder. The second one is the excitonic coherence length⁵⁶:

$$L^{[2]}(t) = \sum_{m \neq n} |\hat{\rho}_{mn}^{el}|, \quad (18)$$

where $\hat{\rho}^{el}$ is the electronic density operator, given by

$$\hat{\rho}^{el} = \sum_R \mathcal{S}_R \cdot \sum_{m,n} (\alpha_m^*(t) \alpha_n(t) |m\rangle \langle n|)_R. \quad (19)$$

Similarly we obtain the third parameter - excitonic coherence length as

$$L_e^{[2]}(t) = \sum_{m \neq n} |\hat{\rho}_{mn}^{exc}|, \quad (20)$$

where $\hat{\rho}_{mn}^{exc}$ is the density operator in the eigenbasis of the electronic Hamiltonian. It represents the quantified amount of coherence between distinct excitonic states. The density operators are normalized according to $\text{Tr} \hat{\rho}^{el} = \text{Tr} \hat{\rho}^{exc} = 1$ condition. In contrast to static models, all parameters are averages of time-dependent stochastic quantities and include the dynamic disorder. The three definitions become very important to investigate the effect of finite temperature on exciton delocalization to isolate the dephasing effects of the thermal environment (see below).

4 Results

The set of parameters is directly taken from our previous papers^{25,29} and in this paper we did not perform any additional fitting of the model parameters. Thus, the direct comparison between the simulation results can be performed. We first calculate the linear polarization and the corresponding absorption spectrum of the full LH2 complex. Using the Eqn. (12), we calculate the dynamics of the system and construct the time-domain optical response function for the ensemble. It decays rapidly on a timescale of ~ 200 fs, so only the initial femtosecond dephasing and energy transfer processes contribute to the absorption spectrum of the system, with later times being relevant only to other spectral signals (such as fluorescence). Absorption spectrum at $T = 100$ K (Fig. 1) reveals the expected double-peak structure with peaks at $\sim 11600 \text{ cm}^{-1}$ and $\sim 12500 \text{ cm}^{-1}$ (see ref.^{23,25,29,57}). The lineshapes and the peak heights calculated using the present variational approach closely match the previous simulations (these were fitted to experiment), which demonstrates that either the Redfield or the present variational simulation approaches do describe the complexity of excitation dynamics relevant to absorption process. Consequently, the set of parameters is sufficiently accurate to describe absorption process.

The electronic excitation causes energy relaxation within the aggregate through both electronic and vibrational degrees of freedom. In the following we proceed to simulate the dynamics in the B850 ring and do not consider the B800. The B850 ring is relevant for, e.g. fluorescence process since only B850 is emitting at long times. Additionally, the excitation dynamics in B850 falls into regime where excitonic interaction

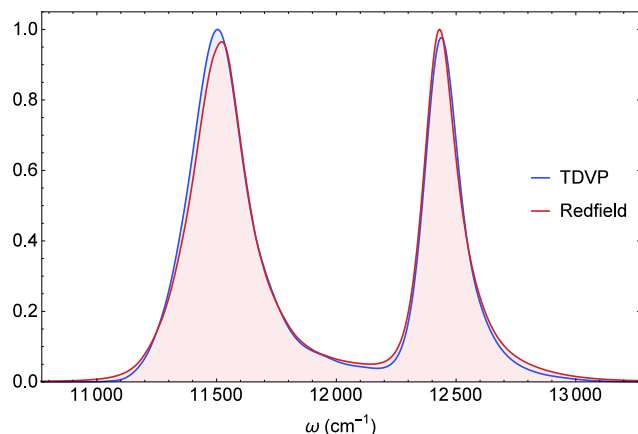


Fig. 1 Absorption spectrum of the full LH2 system at $T = 100$ K. The blue area represents the modeled spectrum using the time-dependent variational approach (TDVP). Averaging over static disorder and thermal fluctuations is performed. The red area is the spectrum calculated with the Redfield approach as described in ref.²⁹.

as well as static and dynamic disorder are of comparable magnitudes. Thus, the excitation dynamics is expected to involve complex polaronic effects.

The population dynamics of B850 ring, shown in Fig. 2, demonstrates a number of expected phenomena in this kind of model, namely energy redistribution among the dimeric subunits of the ring consistent with the kinetic relaxation scheme, and decaying coherent oscillations which can be observed throughout the first 100 fs of evolution.

At all temperatures the duration of the coherent oscillations stays roughly the same, which implies that the dephasing process is dominated by the static disorder instead of the thermal effects. To further reinforce the statement we simulate the dynamics at 100K temperature without the static conformational disorder (Fig. 3). As can be seen, in this case, the coherent oscillations persist up until 500 fs implying that the coherent processes last much longer in a single B850 ring vs. the disordered ensemble. Additionally notice that the final populations weakly depend on temperature and on static disorder. Hence, they must be determined by the energy splitting between various sites and by the intermolecular couplings.

Even though the electronic site populations become quasistationary after 100 fs (with static disorder) or 500 fs (without static disorder), the relaxation process continues due to the evolution of the phase relationships. This is demonstrated by plotting the populations in the excitonic picture (Fig. 4). For the symmetric circular aggregate the lowest energy excitonic state is denoted by quasimomentum $k = 0$, while next two excitonic states are degenerate with $k = \pm 1$. We recover this

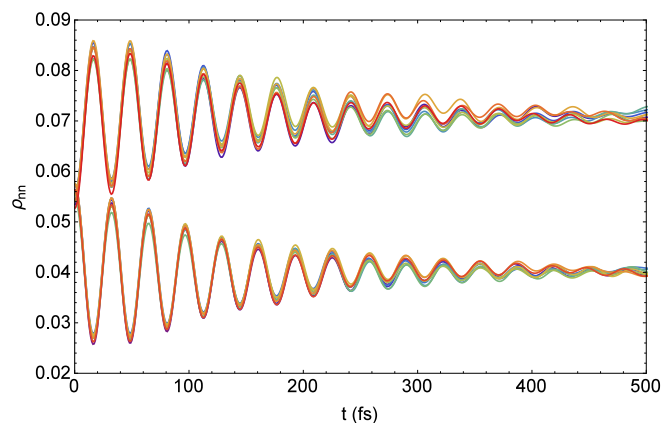


Fig. 3 Time dependencies of site populations of B850 ring at 100 K temperature, with the excitation created by a broadband optical pulse, averaged over thermal fluctuations without static disorder. Different lines represent excitation populations at various sites, $|\alpha_n(t)|^2$ (18 lines totally).

result when static disorder is not included. From Fig. 4 follows that the evolution towards a thermally equilibrated state continues to 2 ps, with the excitonic populations approaching a Boltzmann distribution. For comparison, at $T = 100$ K, $k_B T \approx 70$ cm⁻¹ and the energy gap between apparent $k = 0$ and $k = \pm 1$ states is equal to $\Delta_{k=0, k=\pm 1} = 108$ cm⁻¹. With Boltzmann distribution, $\exp(-\frac{\Delta_{k=0, k=\pm 1}}{k_B T}) \approx 0.21$ which is consistent with the observed asymptotic distributions of the excitonic populations and the excitonic picture (with the second highest excited state populations having approximately 0.2 value). The inclusion of static disorder lifts the degeneracy between $k = +1$ and $k = -1$ states, also slightly slowing down the relaxation process. Higher energy degenerate states $k = \pm 2, 3 \dots$ are similarly split. With the degeneracy lifted we denote the lower and higher energy states correspondingly as $k = 1^-, 2^-, \dots$ for the lower energy states and $k = 1^+, 2^+, \dots$ for the higher energy states. Note that without static disorder we observe slow redistribution of populations in the interval from 1 to 2 ps when the population of the lowest energy excitonic state slightly decreases. This effect implies slow reorganization of excitonic energies which hints on the transition to polaronic states.

Since the polaronic effects seem to appear at ~ 1 ps timescale, auxiliary time-resolved fluorescence (TRF) spectra⁵³ allow us to probe the spectral relaxation dynamics of the system including the complex interplay between the electronic and vibrational degrees of freedom in these timescales. The results at four values of temperature are presented in Fig. 5. We normalize each of the lines to the maximum of the spec-

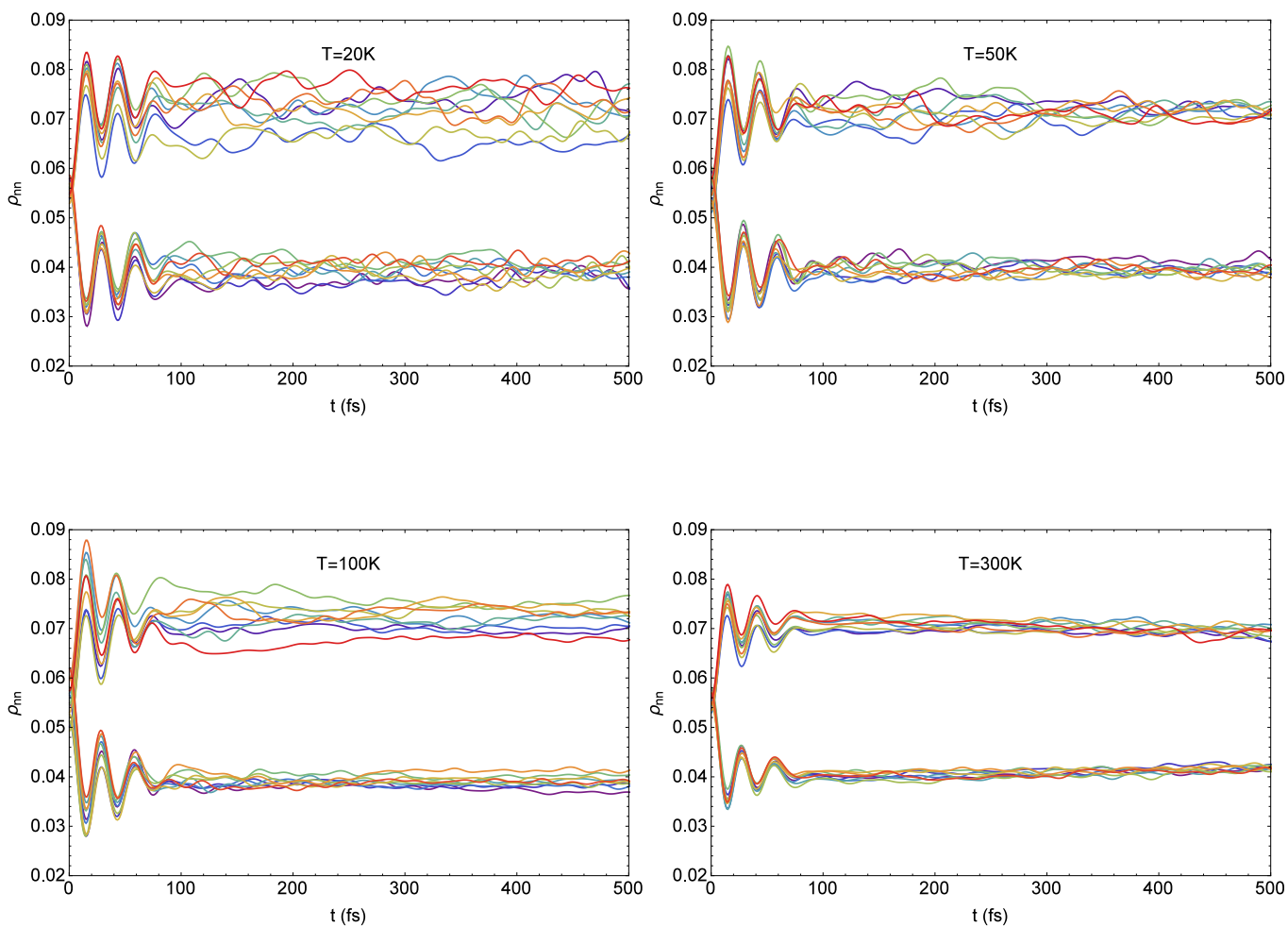


Fig. 2 Time dependencies of site populations of B850 ring at various temperatures, with the excitation created by a broadband optical pulse, averaged over static disorder and thermal fluctuations. Different lines represent excitation populations at various sites, $|\alpha_n(t)|^2$ (18 lines totally).

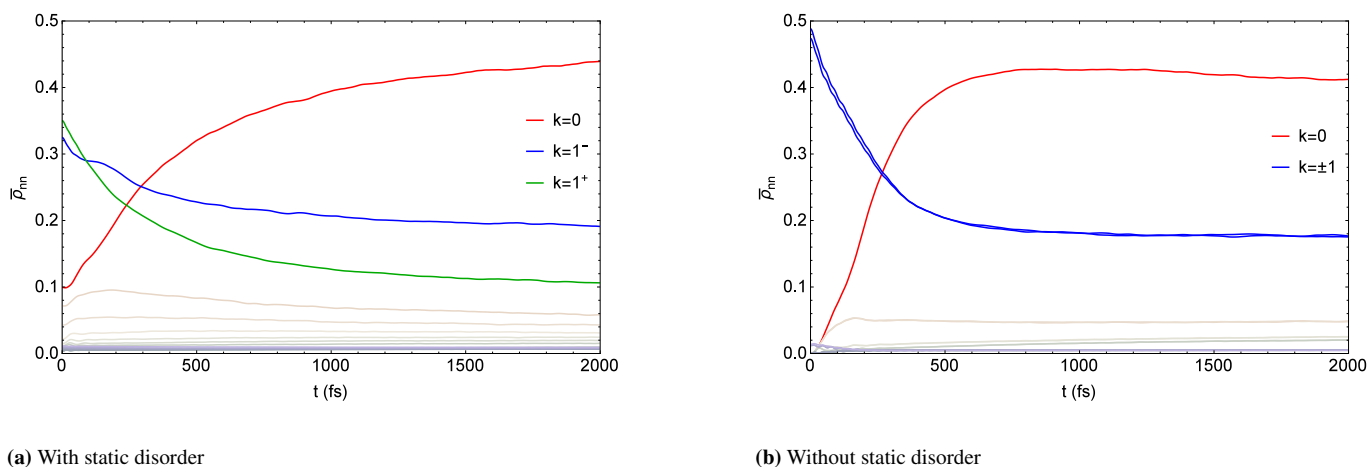


Fig. 4 Time dependencies of excitonic populations as a function of time at $T = 100$ K. We specifically mark the three lowest energy states (labeled by their quasimomentum k in order of increasing energy), the rest of the lines correspond to higher energy states.

trum at $t = 0$.

Some of the features already evident from the site/exciton populations can be seen in the spectra. First, the spectral line at low (20, 50 K) temperatures show fine structure of excitonic bands. At high 300 K temperature the homogeneous broadening becomes larger and excitonic bands become hidden. Second, decay time of the absolute intensity of the spectrum coincides with the decay of coherent effects (Fig. 2), and is attributed first and foremost to the electronic coherence decay process, the second factor playing a role from 500 ps to 1 ps is the relaxation to the $k = 0$ state carrying relatively low dipole strength. This can be clearly seen in the TRF spectra at lower temperatures, where the peak height decays rapidly to a value of about 0.6 during the initial 50 fs, and then relaxation to the $k = 0$ state located at ~ 11400 cm^{-1} redshifts the peak on a slower time scale. At higher temperatures the thermally induced decoherence manifests on a faster time scale, leading to approximately exponential relaxation kinetics (see Fig. 5). Consequently time-resolved fluorescence follows the populations of excitonic states quite accurately and polaronic effects remain difficult to unambiguously identify.

As it turns out with the present set of parameters the polaronic effects remain hidden in the absorption or time-resolved fluorescence spectra. However, to test whether they need to be considered at all we perform the analysis of the wavefunction itself. We thus investigate the exciton participation parameter (Eqn. 17) and the coherence length parameter (Eqn. 18). The exciton participation ratio is calculated separately for each realization and then averaged, thus representing the wavefunction delocalization behaviour for each member in the statistical ensemble. The coherence length is obtained from the elec-

tronic density operator, so it includes the decoherence due to diagonal disorder in a different way.

As can be seen in Figs. 6 and 7, at $t = 0$ the state is highly delocalized due to an excitation by a broadband pulse, with average exciton participation ratio of 11.5 and coherence length of 10.5. Both delocalization parameters, participation ratio $L(t)$ and site coherence length $L^{[2]}(t)$, undergo a small decay in the initial stages of the evolution (~ 100 fs) consistent with the decay of coherences. Then the participation ratio, $L(t)$, decays further at low temperatures, demonstrating characteristics of exciton self-trapping. However, at 300 K temperature the exciton participation starts to slightly increase in value from 500 fs. Overall at 2 ps time the participation grows with temperature. This result suggests that high temperatures counteract the self-trapping, inhibiting the localization process.

The coherence length, $L^{[2]}(t)$, shows a different temperature dependence. It decays rapidly up to 500 fs at all temperatures. It further decays down to ~ 2 at time 2 ps at high 300 K temperature. However at low temperature (20 K) the coherence length grows up to the value of ~ 7 from 500 fs to 2 ps. Thus, the overall picture is the following: at short times both parameters decay together with electronic coherences leading to the primary mixed state formation; later exciton participation grows with temperature, while the coherence length contracts with temperature.

The coherence length not decaying completely and remaining at some fixed value confirms the non-optimality of the site basis. The site basis certainly is not the eigenbasis due to non-zero couplings between sites. Therefore we switch to the excitonic basis and show the coherence length in the excitonic basis set (Eqn. 20) in Fig. 8. Again the length decays within a

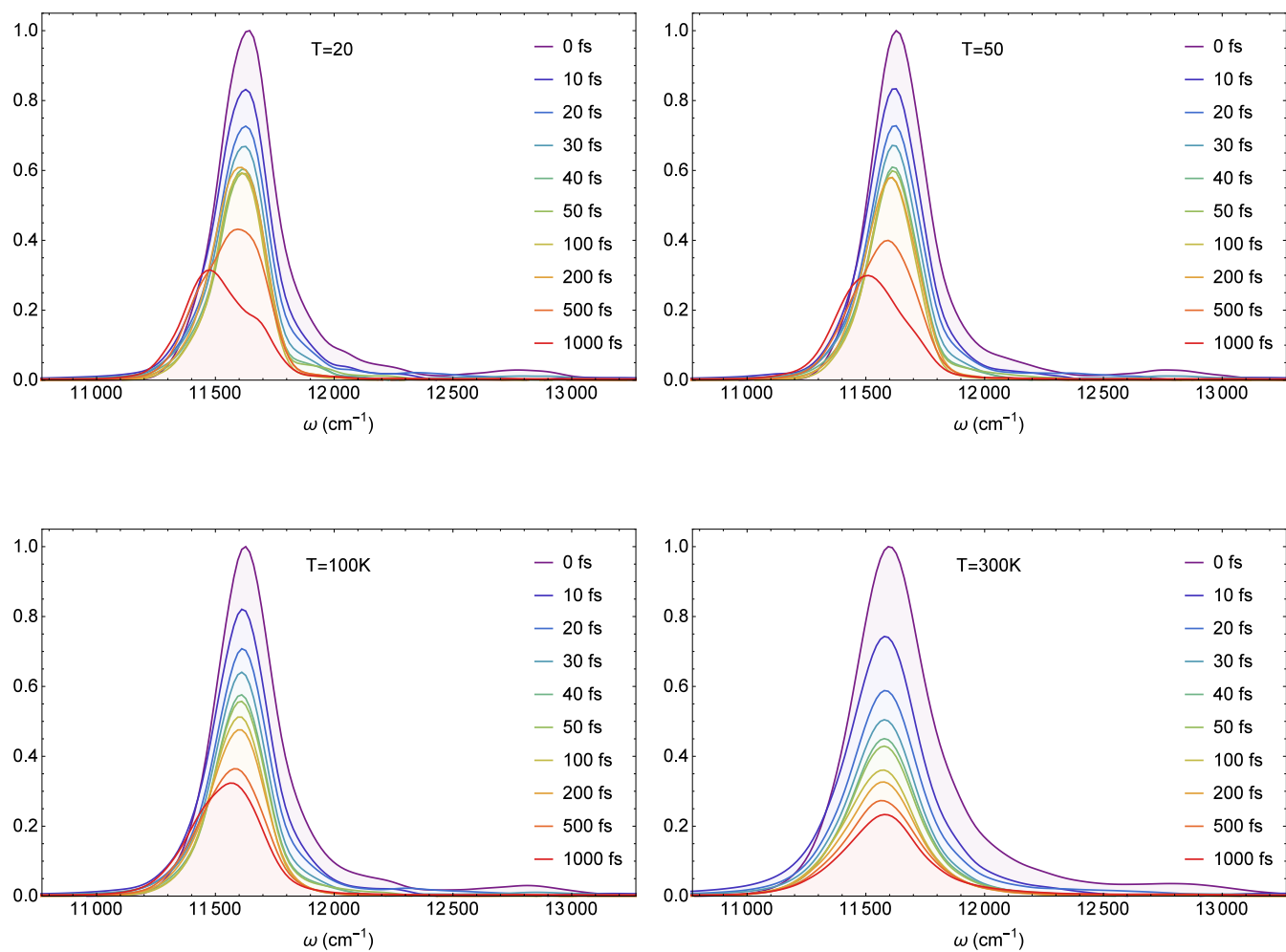


Fig. 5 Time resolved fluorescence spectra of the B850 ring.

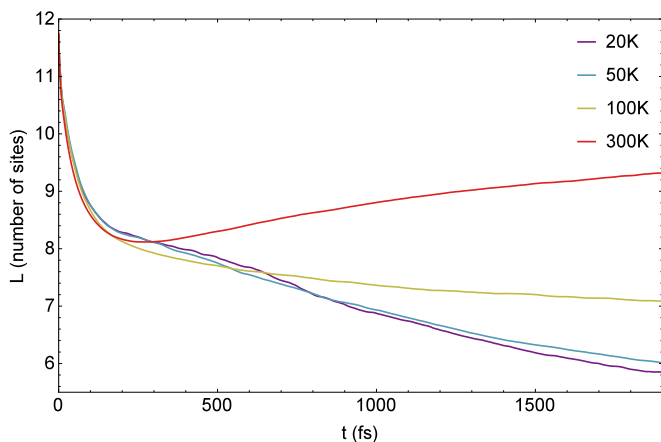


Fig. 6 Time evolution of the participation ratio, $L(t)$, in B850 ring of LH2 aggregate at various temperatures.

few hundred fs in accord with coherence decay and stays constant from 1 ps. Note that asymptotic $L_e^{[2]}(t)$ values are generally much smaller, with the values being lower than 0.5. This implies that the excitonic states are close to the global eigenstates for the system. However, non-zero asymptotic values demonstrate the existence of polaronic effects.

Delocalization parameters demonstrate complicated temperature dependence, which is revealed by the asymptotic values of L , $L^{[2]}$ and $L_e^{[2]}$. This is additional proof of the formation of polaronic picture at temperatures from 20 to 100 K. At 300 K temperature $L_e^{[2]}$ asymptotically decays to zero signifying that only at room temperature the excitonic picture is valid.

5 Discussion

Impact of the thermally fluctuating environment on the properties of the electronic excitations in the molecular aggregates is poorly understood. In the presented stochastic time-dependent variational wavefunction approach a large number of the environmental vibrational modes is treated explicitly and individual trajectories of the excitations with initial stochastic state of the environment at a given temperature can be traced. Thus the environmental effect on the excitation dynamics can be explored in great detail. The distinctive feature of the present approach in comparison to other similar ones^{58,59} is that finite temperature is explicitly included: The energy of initial displacements of the vibrational modes follows a canonical distribution in accord with the statistical physics. Each site is coupled to a separate pool of oscillators, with initial thermal states sampled independently. The presented method is

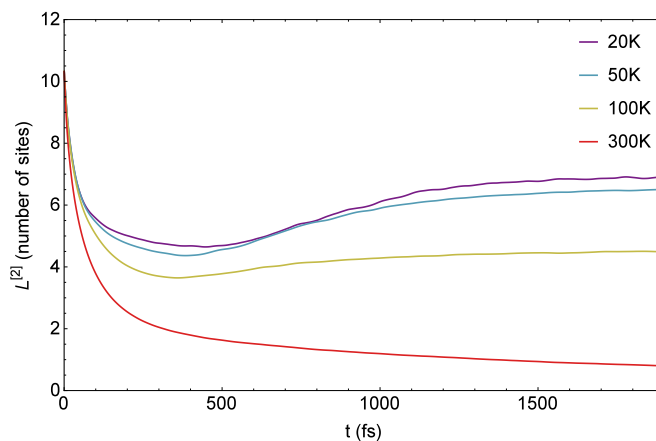


Fig. 7 Time evolution of the coherence length, $L^{[2]}(t)$, in B850 ring of LH2 aggregate at various temperatures.

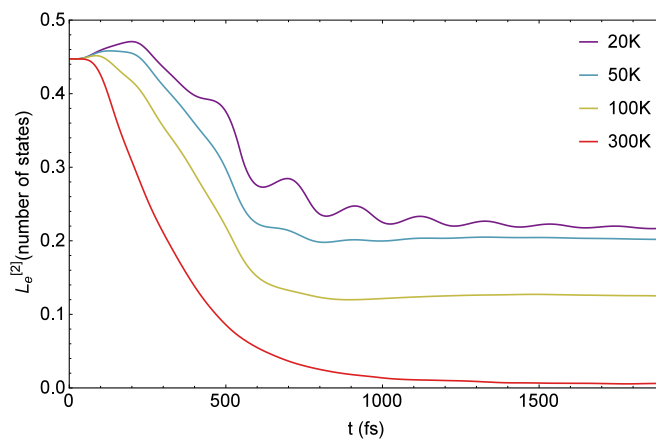


Fig. 8 Time evolution of the coherence length in the excitonic representation, $L_e^{[2]}(t)$, in B850 ring of LH2 aggregate at various temperatures.

non-perturbative, which lets us probe realistic systems where the resonant coupling and the reorganization energy are of the same order, without having to consider one of them as a small perturbation. Also due to the explicit treatment of phonon modes an arbitrary form of spectral density function can be assumed, including both continuous spectral density functions and specific prominent molecular vibrational modes. Timescales of various relaxation processes, attributed to electronic coherence decay caused by static disorder and to influence of the thermal bath can be extracted using the present model, and direct comparison to ultrafast time-resolved spectroscopy experiments can be drawn using the modeled spectra.

LH2 is an ideal object to study the complexity of dissipative excitation dynamics. The approach and parameters are validated by studying absorption (and fluorescence) spectra as well as population dynamics. The energy transfer times within rings of LH2 complexes were experimentally established. The relaxation within B800 ring was estimated to take about 0.3 - 0.4 ps. at all temperatures¹⁸. Fast intraband equilibration of 100 - 200 fs was estimated for the excited states of B850 at 77 K for the LH2 complex of *Rs. molischianum*⁶⁰. Indeed, we obtain a rather similar excitation relaxation and transfer at 100 K (Fig. 4) considering only the B850 ring. The relaxation dynamics in LH2 of *Rb. sphaeroides* at room temperature obtained from the polarization controlled two-dimensional electronic spectroscopy shows 200 fs. component for the relaxation of the B850 high-excited states (identified at 770 nm)²⁶, which is slightly higher than what we observe in our modeled time-resolve fluorescence spectra. This can be partially explained by relaxation pathways involving intramolecular high-frequency molecular vibrations which were not included in our simulations.

An additional property which we can address using our approach is the controversial high-excitonic component of B850 ring^{20,23,55,61}. Keeping the above information, this question thus becomes valid and significant since the excitonic effects at ambient temperatures are apparently highly prominent. The broadband pulse excitation creates populations in the higher energy excitonic states, which manifest themselves as a broad shoulder extending from $\sim 12500\text{ cm}^{-1}$ to $\sim 13000\text{ cm}^{-1}$, and its fast decay during the initial 30 fs of the evolution can be observed (Fig. 5). Its low amplitude makes it difficult to discern in experimental measurements - as expected it is superimposed with the line of the B800 ring in the total spectrum. The high-excitonic component of B850 band was estimated to be at approximately 780 nm (12820 cm^{-1}) for *Rb. sphaeroides* at 77 K²⁰ or near 755 nm (13245 cm^{-1}) at 100 K²³ similarly for *Rb. sphaeroides* and *Rps. acidophila*.

The interplay between excitonic effects and nuclear relaxation can cause evolution of polaronic dynamics and the variational approach includes these effects non-perturbatively. In this paper we show that the polaronic properties do not affect

properties of optical absorption. Its associated spectrum is determined by decay time of linear response function (~ 100 -200 fs). The ultrafast time-resolved fluorescence of LH2 also hardly reveals polaronic properties because its composition reflects structure and symmetry of excitonic energy levels (Figs. 4 and 5).

Therefore we look at intrinsic wavefunction properties. The calculated participation parameter exceeds the corresponding parameter measured in experiments. The exciton delocalization factor of 5 pigments was estimated from the analysis of the LH2 single-complex emission at 1.2 K³⁸. This value is in agreement with the delocalization we obtain at low temperatures. However the simulations of the experimental femtosecond transient absorption and time-dependent pump-probe spectra of bulk LH2 samples performed by different groups suggested the delocalization over 4 - 6 sites around 1 ps. (or steady-state limit) at room temperature and 77 K^{17,62,63}. The authors stayed within the excitonic picture with the Redfield relaxation approximation, thus the delocalization was essentially determined by the interplay of the resonance coupling and the energy disorder in the system. Our previous modeling of nonlinear spectra of LH2 ensemble using Redfield approach²⁹ showed that excitons are delocalized over 3-4 pigments in B850 ring at both 77 K and room temperature as well. These values are significantly smaller than the ones we obtain at corresponding temperatures and delay time for a single realization averaged value in present simulations (Fig. 6). However the present approach is qualitatively different from the ones used in previous work²⁹ and in^{17,62,63}, and allows us to take into account thermal fluctuations already at the wavefunction level.

In essence, the wavefunction of every individual realization (corresponding to single complexes in a medium) is largely delocalized as shown by $L(t)$ parameter. Highly populated sites contribute heavily to the self-trapping effect, leading to the decay of the exciton participation ratio. We find that asymptotic long time values of delocalization parameters are most relevant to inspect the polaronic effects. At low temperatures exciton participation $L(t)$ becomes small denoting self-trapping. At the same time the excitonic coherence length $L_e^{[2]}$ becomes large signifying large departure from excitonic picture. At high temperature the thermal fluctuations impede self-trapping, increasing the delocalization of the wavefunctions. However, this does not imply some kind of different polaron formation, because at high temperature the wavefunction represents a thermally excited superposition of many excitons. The decay of $L_e^{[2]}$ at 300 K on the contrary signifies the validity of the excitonic picture: the resulting wavefunction delocalization in real space is merely due to thermal activation of several excitons. We thus find that proper description of delocalization and polaron formation requires inspection of both participation and coherence parameters simultaneously.

However, whether large participation ratios necessarily correspond to the presence of *coherence* between the pigments is a nontrivial question. Notice that even with large exciton participation ratios at high temperatures in individual rings we do not have large exciton coherence lengths, $L^{[2]}$ (these become even reduced by increasing temperature). This seemingly conflicting result implies fluctuation-induced decoherence process between distant sites inside a single B850 ring: the fluctuations will randomize phase relationships between distant sites in a single wavefunction. We thus observe the decoherence effects within a single B850 ring at large temperature and this explains the temperature-induced reduction of the coherence length.

Actually both parameters demonstrate signatures of excitonic polaron formation. If the picture was purely excitonic, the wavefunction coherence properties must be temperature independent. Now both parameters, $L(t)$ and $L^{[2]}(t)$ demonstrate strong temperature dependence implying transition from temperature-independent excitonic system symmetries to temperature-dependent polaronic picture.

The timescale of polaron formation is yet another important parameter characterizing spectral signature of the polarons. Coherence decay between the wavefunctions in the thermal ensemble (fast decrease of delocalization during first 500 fs) mostly coincides with the decay time of the optical response function and of electronic coherences shown in Fig. 2. These coherences shape the absorption spectrum. This makes the polaronic effects impossible to observe in absorption spectra of the system. The time-resolved fluorescence, according to our simulations, approximately follows excitonic populations. This may be the result of the fact that our long-time coherence length in excitonic basis is considerably smaller than 1, what may be related to our restrictions of the model parameters. Specifically, we did not include the vibration-induced variations of intermolecular couplings. This is the major cause of exciton self-trapping observed by the temperature dependence of the fluorescence lifetime^{21,55} in real photosynthetic aggregates.

While not studied in this paper, the delocalization depends on the specific spectral content of bath fluctuations. If the bath fluctuations are very slow, as demonstrated in⁴², the wavefunction becomes adiabatically trapped by energy deformation. More specifically, the slow phonon modes act as quasi-static disorder and hence necessarily localize the excitonic wave function in the Anderson sense, i. e. the disorder parametrically or adiabatically localizes quantum particles. Thus, the localization does not necessarily involve response of vibrational coordinates to the excitation or the feedback of interaction. Simple thermal fluctuations will induce localization. Consequently higher temperature will cause more localization. If the high frequency molecular vibrations are in place, the polaronic effects mostly manifest due to feedback action.

In this case the higher temperature will cause detrapping. In the present simulations we observe thermal detrapping. The effect is due to thermal reduction of interaction feedback, thus our vibrational modes are in high frequency regime.

The vibrational frequencies strongly overlap with excitonic energy splittings and thermal energy $k_B T$. Overlapping energies allow strong mixing of electronic and vibrational degrees of freedom, while thermal activation leads to the vibronic dynamics. Finally, this phenomenon may assist fast relaxation between energy bands in LH2 and fast exciton transport in other photosynthetic systems.

There is another temperature-related issue that should not be ignored while describing realistic LH2 aggregates. Numerous experiments and modeling show that various system and environment related parameters of LH2 complex depend on temperature and this dependence is not simply linear^{23,29,33,55,64}. The present model is therefore not fully comprehensive to accommodate all features of LH2 aggregate^{54,65,66}. The parameters used in the present modeling are those previously determined for 100 K temperature²⁹. Consequently, the direct comparison of the results presented here with those obtained elsewhere for LH2 complex is tenable only for 100 K. We intentionally keep the same parameters at all temperatures in order to reveal the manifestation of the temperature effects in the properties of the wavefunction.

6 Conclusions

We presented a stochastic variational wavefunction approach describing excitation dynamics in a large molecular aggregate. Our approach allows arbitrary geometries, various environmental properties and also takes into account the impact of the electronic excitation in the system on the local vibrational environment. In contrast to other applications of the variational wavefunction approach, which consider the zero-temperature case^{58,59}, we simulate the dynamics at finite temperatures by randomly sampling initial amplitudes of vibrational modes. The theory is applied to model the energy transfer within the B850 ring of the LH2 photosynthetic complex. The modeled results demonstrate that polaronic effects are small in optical absorption and fluorescence spectra. However, the dependence of wavefunction delocalization parameters $L(t)$, $L^{[2]}(t)$ and $L_e^{[2]}(t)$ and especially their asymptotic values signify transition to temperature-dependent polaronic picture.

A Derivation of the equations of motion

In this appendix we present the derivation of equations of motion used in this paper. Starting from the Lagrangian of the system

$$\mathcal{L} = \frac{i}{2} \left(\langle \Psi_{D_2}(t) | \dot{\Psi}_{D_2}(t) \rangle - \langle \dot{\Psi}_{D_2}(t) | \Psi_{D_2}(t) \rangle \right) - \langle \Psi_{D_2}(t) | \hat{H} | \Psi_{D_2}(t) \rangle \quad (21)$$

we can derive the equations of motion using the Euler-Lagrange equations for the set of variational parameters which parametrize the Davydov D_2 Ansatz $\{\alpha_n^*(t), \lambda_q^*(t)\}$:

$$\frac{d}{dt} \left(\frac{\partial \mathcal{L}}{\partial \dot{\alpha}_n^*} \right) - \frac{\partial \mathcal{L}}{\partial \alpha_n^*} = 0, \quad \forall n, \quad (22)$$

$$\frac{d}{dt} \left(\frac{\partial \mathcal{L}}{\partial \dot{\lambda}_q^*} \right) - \frac{\partial \mathcal{L}}{\partial \lambda_q^*} = 0, \quad \forall q. \quad (23)$$

First we calculate the time derivative of the D_2 trial wavefunction

$$\begin{aligned} |\dot{\Psi}_{D_2}(t)\rangle &= \sum_n \left\{ \dot{\alpha}_n \hat{a}_n^\dagger \exp \left(\sum_q \lambda_q \hat{b}_q^\dagger - \text{h.c.} \right) \right. \\ &\quad \left. + \alpha_n \hat{a}_n^\dagger \sum_q \left[\left(\dot{\lambda}_q \hat{b}_q^\dagger - \text{h.c.} \right) - \frac{1}{2} \left(\dot{\lambda}_q \lambda_q^* - \text{c.c.} \right) \right] \right. \\ &\quad \left. \cdot \exp \left(\sum_q \lambda_q \hat{b}_q^\dagger - \text{h.c.} \right) \right\} |0\rangle. \end{aligned} \quad (24)$$

Calculating the expression $\frac{i}{2} \left(\langle \Psi_{D_2}(t) | \dot{\Psi}_{D_2}(t) \rangle - \langle \dot{\Psi}_{D_2}(t) | \Psi_{D_2}(t) \rangle \right)$, we obtain the kinetic part of the Lagrangian:

$$\mathcal{K} = \frac{i}{2} \sum_n \left\{ \dot{\alpha}_n \alpha_n^* - \dot{\alpha}_n^* \alpha_n + \alpha_n \alpha_n^* \left(\dot{\lambda}_q \lambda_q^* - \text{c.c.} \right) \right\}. \quad (25)$$

The potential part is expressed as the scalar product $\langle \Psi_{D_2}(t) | \hat{H} | \Psi_{D_2}(t) \rangle$ and is equal to:

$$\begin{aligned} \mathcal{U} &= \sum_n (\varepsilon_n + \delta_n) |\alpha_n|^2 + \sum_{m \neq n} J_{mn} \alpha_n^* \alpha_m \\ &\quad + \sum_n |\alpha_n|^2 \sum_q \omega_q |\lambda_q|^2 - \sum_n |\alpha_n|^2 \sum_q g_{qn} \omega_q (\lambda_q + \lambda_q^*). \end{aligned} \quad (26)$$

The explicit expression for the Lagrangian is then

$$\begin{aligned} \mathcal{L} &= \frac{i}{2} \sum_n \left\{ \dot{\alpha}_n \alpha_n^* - \dot{\alpha}_n^* \alpha_n + \alpha_n \alpha_n^* \left(\dot{\lambda}_q \lambda_q^* - \text{c.c.} \right) \right\} \\ &\quad - \sum_n (\varepsilon_n + \delta_n) |\alpha_n|^2 - \sum_{m \neq n} J_{mn} \alpha_n^* \alpha_m \\ &\quad - \sum_n |\alpha_n|^2 \sum_q \omega_q |\lambda_q|^2 + \sum_n |\alpha_n|^2 \sum_q g_{qn} \omega_q (\lambda_q + \lambda_q^*). \end{aligned} \quad (27)$$

Inserting it into the Euler-Lagrange equations (22), (23) and simplifying the result, assuming the single-excitation condition $\sum_n |\alpha_n|^2 = 1$ we obtain the equations

$$\begin{aligned} \dot{\alpha}_n &= -i \alpha_n \sum_{n,q} |\alpha_n|^2 g_{qn} \omega_q (\lambda_q + \lambda_q^*) - i \sum_m J_{mn} \alpha_m \\ &\quad + i \alpha_n \sum_q g_{qn} \omega_q (\lambda_q + \lambda_q^*), \\ \dot{\lambda}_q &= -i \omega_q \lambda_q + i \sum_n |\alpha_n|^2 g_{qn} \omega_q. \end{aligned}$$

Inserting the definition of the collective coordinate (Eqn. 5), we immediately arrive at the final Eqns. (3), (4).

References

- H. van Amerongen, L. Valkunas and R. van Grondelle, *Photosynthetic Excitons*, World Scientific, Singapore, New Jersey, London, Hong Kong, 2006, p. 590.
- R. Blankenship, *Molecular Mechanisms of Photosynthesis*, Wiley, 2014.
- L. Valkunas, D. Abramavicius and T. Mančal, *Molecular Excitation Dynamics and Relaxation*, Wiley-VCH Verlag GmbH & Co. KGaA, Weinheim, Germany, 2013.
- D. Abramavicius and L. Valkunas, *Photosynth. Res.*, 2015, 1–15.
- M. Schröter, S. Ivanov, J. Schulze, S. Polyutov, Y. Yan, T. Pullerits and O. Kühn, *Phys. Rep.*, 2015, **567**, 1 – 78.
- F. C. Spano, *Acc. Chem. Res.*, 2010, **43**, 429–439.
- R. Jankowiak, M. Reppert, V. Zazubovich, J. Pieper and T. Reinot, *Chem. Rev.*, 2011, **111**, 4546–4598.
- A. Gall, A. A. Pascal and B. Robert, *Biochim. Biophys. Acta*, 2015, **1847**, 12–18.
- F. D. Fuller and J. P. Ogilvie, *Annu. Rev. Phys. Chem.*, 2015, **66**, 667–690.
- R. J. Cogdell, A. Gall and J. Köhler, *Q. Rev. Biophys.*, 2006, **39**, 227–324.
- X. Hu, T. Ritz, A. Damjanovic, F. Autenrieth and K. Schulten, *Q. Rev. Biophys.*, 2002, **35**, 1–62.
- G. McDermott, S. Prince, A. Freer, A. Hawthornthwaite-Lawless, M. Papiz, R. Cogdell and N. Isaacs, *Nature*, 1995, **374**, 517–521.
- J. Koepke, X. Hu, C. Muenke, K. Schulten and H. Michel, *Structure*, 1996, **4**, 581–597.
- S. Prince, M. Papiz, A. Freer, G. McDermott, A. Hawthornthwaite-Lawless, R. Cogdell and N. Isaacs, *J. Mol. Biol.*, 1997, **268**, 412–423.
- M. Papiz, S. Prince, T. Howard, R. Cogdell and N. Isaacs, *J. Mol. Biol.*, 2003, **326**, 1523–1538.
- J. F. Imhoff, *Int. J. Syst. Evol. Microbiol.*, 2001, **51**, 1863.
- T. Pullerits, M. Chachisvilis and V. Sundström, *J. Phys. Chem.*, 1996, **100**, 10787–10792.
- V. Sundström, T. Pullerits and R. van Grondelle, *J. Phys. Chem. B*, 1999, **103**, 2327–2346.
- G. D. Scholes and G. R. Fleming, *J. Phys. Chem. B*, 2000, **104**, 1854–1868.
- M. Ketelaars, A. M. van Oijen, M. Matsushita, J. Köhler, J. Schmidt and T. J. Aartsma, *Biophys. J.*, 2001, **80**, 1591–1603.
- A. Freiberg, M. Rätsep, K. Timpmann, G. Trinkunas and N. W. Woodbury, *J. Phys. Chem. B*, 2003, **107**, 11510–11519.
- Y. C. Cheng and R. J. Silbey, *Phys. Rev. Lett.*, 2006, **96**, 028103.
- G. Trinkunas, O. Zerlauskienė, V. Urbonienė, J. Chmeliov, A. Gall, B. Robert and L. Valkunas, *J. Phys. Chem. B*, 2012, **116**, 5192–5198.
- R. J. Cogdell and J. Köhler, *Biochem. J.*, 2009, **422**, 193–205.

- 25 O. Rancova, J. Sulskus and D. Abramavicius, *J. Phys. Chem. B*, 2012, **116**, 7803–7814.
- 26 A. F. Fidler, V. P. Singh, P. D. Long, P. D. Dahlberg and G. S. Engel, *J. Chem. Phys.*, 2013, **139**, 155101.
- 27 A. F. Fidler, V. P. Singh, P. D. Long, P. D. Dahlberg and G. S. Engel, *J. Phys. Chem. Lett.*, 2013, **4**, 1404–1409.
- 28 A. F. Fidler, V. P. Singh, P. D. Long, P. D. Dahlberg and G. S. Engel, *Nat. Commun.*, 2014, **5**, year.
- 29 O. Rancova and D. Abramavicius, *J. Phys. Chem. B*, 2014, **118**, 7533–7540.
- 30 H.-M. Wu, N. R. S. Reddy, and G. J. Small*, *J. Phys. Chem. B*, 1997, **101**, 651–656.
- 31 F. v. M. Rene Monshouwer, Malin Abrahamsson and R. van Grondelle, *J. Phys. Chem. B*, 1997, **101**, 7241–7248.
- 32 A. M. van Oijen, M. Ketelaars, J. Köhler, T. J. Aartsma and J. Schmidt, *Science*, 1999, **285**, 400–402.
- 33 J. Meldaikis, O. Zerlauskienė, D. Abramavicius and L. Valkunas, *Chem. Phys.*, 2013, **423**, 9–14.
- 34 O. Zerlauskienė, G. Trinkunas, A. Gall, B. Robert, V. Urbonienė and L. Valkunas, *J. Phys. Chem. B*, 2008, **112**, 15883–15892.
- 35 T. Polívka, T. Pullerits, J. L. Herek and V. Sundström, *J. Phys. Chem. B*, 2000, **104**, 1088–1096.
- 36 K. Timpmann, Z. Katiliene, N. W. Woodbury and A. Freiberg, *J. Phys. Chem. B*, 2001, **105**, 12223–12225.
- 37 A. Freiberg, M. Rätsep, K. Timpmann and G. Trinkunas, *Chem. Phys.*, 2009, **357**, 102–112.
- 38 R. Kunz, K. Timpmann, J. Southall, R. J. Cogdell, A. Freiberg and J. Köhler, *J. Phys. Chem. B*, 2012, **116**, 11017–11023.
- 39 A. Gelzinis, D. Abramavicius and L. Valkunas, *Phys. Rev. B*, 2011, **84**, 245430.
- 40 W. H. Zurek, *Phys. Rev. D*, 1981, **24**, 1516–1525.
- 41 E. Joos and H. D. Zeh, *Z. Phys. B*, 1985, **59**, 223–243.
- 42 V. Chorosajev, A. Gelzinis, L. Valkunas and D. Abramavicius, *J. Chem. Phys.*, 2014, **140**, 244108.
- 43 S. R. White and R. M. Noack, *Phys. Rev. Lett.*, 1992, **68**, 3487–3490.
- 44 J. Sun, L. Duan and Y. Zhao, *J. Chem. Phys.*, 2013, **138**, 174116.
- 45 J. Sun, B. Luo and Y. Zhao, *Phys. Rev. B*, 2010, **82**, 014305.
- 46 B. Luo, J. Ye and Y. Zhao, *Phys. Status Solidi (c)*, 2011, **8**, 70–73.
- 47 M. J. Skrinjar, D. V. Kapor and S. D. Stojanovic, *Phys. Rev. A*, 1988, **38**, 6402–6408.
- 48 B. Luo, J. Ye, C. Guan and Y. Zhao, *Phys. Chem. Chem. Phys.*, 2010, **12**, 15073–15084.
- 49 V. May and O. Kühn, *Charge and Energy Transfer Dynamics in Molecular Systems*, Wiley-VCH Verlag GmbH & Co. KGaA, Weinheim, Germany, 2011, p. 562.
- 50 I. Frenkel and J. Frenkel, *Wave Mechanics: Elementary Theory*, Oxford University Press, 1936.
- 51 D. Walls and G. Milburn, *Quantum Optics*, Springer Berlin Heidelberg, 2008.
- 52 S. S. Mukamel, *Principles of nonlinear optical spectroscopy*, New York : Oxford University Press, 1995.
- 53 V. Balevičius Jr., L. Valkunas and D. Abramavicius, *J. Chem. Phys.*, 2015, **143**, year.
- 54 O. Rancova, R. Jankowiak and D. Abramavicius, *J. Chem. Phys.*, 2015, **142**, 212428.
- 55 M. Pajusalu, M. Rätsep, G. Trinkunas and A. Freiberg, *ChemPhysChem*, 2011, **12**, 634–644.
- 56 T. Meier, Y. Zhao, V. Chernyak and S. Mukamel, *J. Chem. Phys.*, 1997, **107**, 3876–3893.
- 57 S. Georgakopoulou, R. N. Frese, E. Johnson, C. Koolhaas, R. J. Cogdell, R. van Grondelle and G. van der Zwan, *Biophys. J.*, 2002, **82**, 2184.
- 58 J. Ye, K. Sun, Y. Zhao, Y. Yu, C. K. Lee and J. Cao, *J. Chem. Phys.*, 2012, **136**, 245104.
- 59 K. Sun, J. Ye and Y. Zhao, *J. Chem. Phys.*, 2014, **141**, 124103.
- 60 V. Novoderezhkin, M. Wendling and R. van Grondelle, *J. Phys. Chem. B*, 2003, **107**, 11534–11548.
- 61 M. H. C. Koolhaas, R. N. Frese, G. J. S. Fowler, T. S. Bibby, S. Georgakopoulou, G. van der Zwan, C. N. Hunter and R. van Grondelle, *Biochemistry (Mosc.)*, 1998, **37**, 4693.
- 62 R. van Grondelle and V. Novoderezhkin, *Biochemistry (Mosc.)*, 2001, **40**, 15057–15068.
- 63 M. Dahlbom, T. Pullerits, S. Mukamel and V. Sundström, *J. Phys. Chem. B*, 2001, **105**, 5515–5524.
- 64 H.-M. Wu, M. Rätsep, R. Jankowiak, R. J. Cogdell and G. J. Small, *J. Phys. Chem. B*, 1997, **101**, 7641–7653.
- 65 D. Hsu and J. L. Skinner, *J. Chem. Phys.*, 1984, **81**, 1604.
- 66 J. L. Skinner and D. Hsu, *J. Phys. Chem.*, 1986, **90**, 4931–4938.